Redox Biology 40 (2021) 101856

Contents lists available at ScienceDirect

Redox Biology

journal homepage: www.elsevier.com/locate/redox

Research Paper

Heat shock protein 22 modulates NRF1/TFAM-dependent mitochondrial biogenesis and DRP1-sparked mitochondrial apoptosis through AMPK-PGC1α signaling pathway to alleviate the early brain injury of subarachnoid hemorrhage in rats

Haiyan Fan [a,1], Rui Ding [c,1], Wenchao Liu [a], Xin zhang [a], Ran Li [a], Boyang Wei [a], Shixing Su [a], Fa Jin [a], Chengcong Wei [a], Xuying He [a], Xifeng Li [a,**], Chuanzhi Duan [a,b,*]

[a] Neurosurgery Center, Department of Cerebrovascular Surgery, Engineering Technology Research Center of Education Ministry of China on Diagnosis and Treatment of Cerebrovascular Disease, Zhujiang Hospital, Southern Medical University, Guangzhou, 510280, Guangdong, China
[b] Guangdong Provincial Key Laboratory on Brain Function Repair and Regeneration, 510280, Guangdong, China
[c] Department of Cerebrovascular Surgery, The Third Affiliated Hospital, Sun Yat-Sen University, Guangzhou, 510630, Guangdong, China

ARTICLE INFO

Keywords:
Heat shock protein 22
Mitochondria
AMPK-PGC1α
Subarachnoid hemorrhage

ABSTRACT

Mitochondrial dysfunction has been widely accepted as a detrimental factor in subarachnoid hemorrhage (SAH)-induced early brain injury (EBI), which is eminently related to poor neurologic function outcome. Previous studies have revealed that enhancement of heat shock protein 22 (hsp22) under conditions of stress is a friendly mediator of mitochondrial homeostasis, oxidative stress and apoptosis, thus accelerating neurological recovery. However, no study has confirmed whether hsp22 attenuates mitochondrial stress and apoptosis in the setting of SAH-induced EBI. Our results indicated that endogenous hsp22, p-AMPK/AMPK, PGC1α, TFAM, Nrf1 and Drp1 were significantly upregulated in cortical neurons in response to SAH, accompanied by neurologic impairment, brain edema, neuronal degeneration, lower level of mtDNA and ATP, mitochondria-cytosol translocation of cytochrome c, oxidative injury and caspase 3-involved mitochondrial apoptosis. However, exogenous hsp22 maintained neurological function, reduced brain edema, improved oxidative stress and mitochondrial apoptosis, these effects were highly dependent on PGC1α-related mitochondrial biogenesis/fission, as evidenced by co-application of PGC1α siRNA. Furthermore, we demonstrated that blockade of AMPK with dorsomorphin also compromised the neuroprotective actions of hsp22, along with the alterations of PGC1α and its associated pathway molecules. These data revealed that hsp22 exerted neuroprotective effects by salvaging mitochondrial function in an AMPK-PGC1α dependent manner, which modulates TFAM/Nrf1-induced mitochondrial biogenesis with positive feedback and DRP1-triggered mitochondrial apoptosis with negative feedback, further reducing oxidative stress and brain injury. Boosting the biogenesis and repressing excessive fission of mitochondria by hsp22 may be an efficient treatment to relieve SAH-elicited EBI.

1. Introduction

Subarachnoid hemorrhage (SAH), a severe stroke subtype, is mainly caused by aneurysm rupture[1,2] with high morbidity and mortality and remaining neurological deficits [3]. Transient global ischemia and local blood invasiveness after SAH will restrain oxidative phosphorylation, elicit mitochondrial homeostasis disorders and reactive oxygen species (ROS) storm [4], which are detrimental for neuronal viability and development [5]. Over the past decades, mitochondria have been well recognized as major regulators that control neurological function and neuron viability under SAH [6,7].

It is ascertained that mitochondria not only are the main site of ATP

* Corresponding author. Department of Cerebrovascular Surgery, Neurosurgery Center, Zhujiang Hospital, Southern Medical University, No.253. Gongye Middle Avenue, Haizhu District, Guangzhou, 510280, Guangdong, China.
** Corresponding author.
E-mail addresses: nflxf@126.com (X. Li), doctor_duanzj@163.com (C. Duan).
[1] Haiyan Fan and Rui Ding contributed equally.

https://doi.org/10.1016/j.redox.2021.101856
Received 21 October 2020; Received in revised form 14 December 2020; Accepted 31 December 2020
Available online 6 January 2021

production but also participate in the ROS formation and cell apoptosis [8,9]. Importantly, accumulating evidence has indicated that mitochondrial biogenesis and fusion/fission play crucial roles in maintaining mitochondrial function and homeostasis [5]. Concretely, the biogenesis sustains mitochondrial DNA(mtDNA) replication, modulates oxidative phosphorylation, boosting ATP generation [10]. In contrast to biogenesis, excessive mitochondrion fission will break mitochondrial homeostasis, leading to the production of inundant ROS [11] and the translocation of cytochrome C into cytoplasm [12], thereby igniting apoptosis [13]. Also, more robust data concerning the favorable effects exerted by modulation of mitochondrial biogenesis/fission have been validated in cerebral ischemia [9], diabetes-accelerated atherosclerosis [11] and Dox-induced cardiotoxicity [13]. Consequently, specific tactics urgently need to be introduced to strengthen the biogenesis and interrupt excessive fission of mitochondria to attenuate the EBI after SAH.

Heat shock protein 22 (Hsp22), also called H11 Kinase and HSPB8, is a small heat shock protein and originally as a necessity for the growth of *Drosophila melanogaster* [14,15], has recently been demonstrated to have the properties of mitochondria-protection, anti-oxidation, anti-apoptosis in myocardial injury [16], cerebral ischemia [17] and aging [18]. Notably, hsp22 treatment could maintain the balance of mitochondrial fusion and fission to mitigate mitochondria-derived ROS [19]. Additionally, forceful proofs demonstrated that overexpression of hsp22 markedly attenuates oxidative stress-induced hippocampal neuronal cell death through the suppression of mitochondria-mediated apoptosis cascade responses [20]. Reciprocally, silencing hsp22 remarkably aggravates mitochondrial impairment via repression of oxidative phosphorylation and accompanying ATP production [21]. Considering the vital role of mitochondria in EBI after SAH, it is tempting to speculate that whether the upregulation of hsp22 may ameliorate SAH-mediated EBI via the boosting of the biogenesis and the suppression of excessive division of mitochondria. Nevertheless, the exact underlying mechanism of how hsp22 improves mitochondrial dysfunction remains scarce.

Adenosine 5'monophosphate-activated protein kinase (AMPK), as a cellular energy sensor, is a trimer composed of α, β and γ subunit units. Potent evidence displayed that activation of AMPK at the site of Thr172 could modulate mitochondrial biogenesis and fission [22,23], reduce ROS [24,25] and mitigate cell apoptosis [26] in various pathological processes. Moreover, the co-immunoprecipitation assay substantiated that hsp22 can diminish myocardial ischemia injury by promoting the Thr172 phosphorylation of AMPK [27]. Surprisingly, it is reported that recently, in the SAH rat model, activating AMPK exerts its neuroprotective effects via the inhibition of oxidative stress [28]. Momentously, at the molecular levels, AMPK up-regulates peroxisome proliferative activated receptor γ (PPARγ) coactivator 1α (PGC1-α), which is also confirmed to be intimately relevant to the promotion of mitochondrial biogenesis [9] and inhibition of mitochondrial fission [29]. Along with the well-documented role played by AMPK-PGC1α-related mitochondrial biogenesis and fission, it is extremely worthwhile to explore whether AMPK-PGC1α signaling is implicated in the regulatory effects of hsp22 on mitochondrial function.

Therefore, the purpose of this study was (i) to define whether Hsp22 alleviates SAH-induced EBI via the modulation of NRF1/TFAM-dependent mitochondrial biogenesis and DRP1-mediated mitochondrial apoptosis, and amelioration of oxidative stress and brain injury; (ii) if so, to investigate whether Hsp22 ameliorates the mitochondrial abnormality via the activation of AMPK-PGC1α signaling. Using in vivo SAH rat model, our results demonstrate that Hsp22 promotes mitochondrial biogenesis and prevents excessive mitochondrial fission in an AMPK-PGC1α-dependent manner in SAH.

2. Materials and methods

2.1. Animal models of SAH

This study was conducted in accordance with the guideline for the care and use of laboratory animals published by the US national institutes of health. All experimental protocols were approved by the Ethics Committee of Zhujiang Hospital of Southern Medical University. Adult male Sprague-Dawley rats weighing 290–310g, obtained from the Animal Experiment Center of Southern Medical University, were employed to induce endovascular perforation SAH model according to the methods of our previous study [30]. The same procedure was performed in the sham group without intravascular puncture.

2.1.1. Experimental group design (Supplemental Fig. 1)

2.1.1.1. Experiment 1. 42 rats were randomly allocated into the seven groups including the sham group and six SAH subgroups (at 3 h, 6 h, 12 h, 24 h, 48 h, 72 h after SAH. n = 6) for the Western blot detection of the dynamic alterations of Hsp22. Besides, 4 rats were evenly distributed to sham and SAH (n = 2 per group) for the cellular localization of Hsp22 by double fluorescent staining.

2.1.1.2. Experiment 2. 60 rats were randomly divided into the five groups including sham, SAH + vehicle, SAH + hsp22 (3 μg/kg), SAH + hsp22 (10 μg/kg) and SAH + hsp22 (30 μg/kg) for the examination of neurological scoring (n = 6), brain water content (BWC) (n = 6), Terminal deoxynucleotidyl transferase dUTP nick end labeling (TUNEL) staining (n = 4), FJC staining (n = 4), Western blot (WB, n = 6), and immunofluorescence (IF) staining (n = 4). Based on the above experimental results, the optimal dose of HSP22 (10 μg/kg) was selected for subsequent experiments. Afterward, 32 rats were equally allocated into the two groups (n = 16) including SAH + scramble siRNA and SAH + hsp22 siRNA for neurological scoring (n = 6), BWC (n = 6), FJC staining (n = 4), Western blot (WB, n = 6) and immunofluorescence (IF) staining (n = 4).

2.1.1.3. Experiment 3. 170 rats were randomly assigned into the five groups including sham, SAH + vehicle, SAH + hsp22, SAH + hsp22+Scramble siRNA, SAH + hsp22 + PGC1α siRNA for the tests of neurological scoring (n = 6), BWC (n = 6), TUNEL (n = 4), IF (n = 4), IHC (n = 4), ATP content (n = 6), enzyme-linked immunosorbent assay (ELISA, n = 6), mtDNA (n = 6), DHE (n = 4), transmission electron microscopy (TEM, n = 4) and WB (n = 6).

2.1.1.4. Experiment 4. 16 rats were allocated into SAH + hsp22 + Dorsomorphin for the tests of neurological scoring (n = 6), BWC (n = 6), WB (n = 6), TUNEL (n = 4) and IF staining (n = 4).

2.2. Drug administration

The hsp22 recombinant protein, dorsomorphin and vehicle were injected into the lateral ventricle at 0.5 h after SAH ictus. Hsp22 siRNA, PGC1α siRNA and scramble siRNA were injected into the lateral ventricle at 48 h before SAH induction.

2.3. Neurological score evaluation

The modified Garcia scoring system and beam balance test was utilized to assess the neurological function by two blinded observer at 24 h after SAH, as formerly reported. Simply put, the modified Garcia test is comprised of six sub-tests: three of which have a score of 0–3, including spontaneous activity, symmetry of limb movement and forelimb extension. The other three tests scored 1–3, encompassing climbing ability, body proprioception and response to vibration stimulation. The

total score ranged from 3 to 18. The beam balance test was performed to evaluate the ability of rats to walk on a 15-mm-wide wooden beam lasting for 1 min. The mean score was computed according to three consecutive trials scored from 0 to 4 on the basis of the walking ability. Higher scores are parallel to better neurological function.

2.4. SAH grade

The SAH grade was employed to assess the severity of SAH by an independent observer who was blind to the experiment as previously depicted. Simply put, the basal of the rat brain is divided into six subsections. Each section was scored on a scale of 0–3 in terms of the size of the subarachnoid clot. Rats with mild SAH (SAH grade $\leq$7) were eliminated.

2.5. Brain water content

After anesthetized and decapitated, rat brains were rapidly removed and separated into four parts in the light of the left brain, right brain, cerebellum and brain stem at 24 h post-SAH. Each part was directly weighed to obtain wet weight and then dried in a 105 °C oven for 48 h to acquire dry weight. The percentage of BWC was calculated as [(wet weight − dry weight)/wet weight] × 100%.

2.6. Hematoxylin-eosin staining

Rats were transcardially perfused with 500 ml 4% paraformaldehyde at 24 h after SAH, as formerly reported. After fixation in 4% paraformaldehyde, dehydration, and paraffin-embedding, 4 μm-thickness consecutive coronary sections of rat brain were prepared. After dewaxing, the sections were stained with H&E solution according to a commercial kit (C0105S, Beyotime Biotechnology, China).

2.7. Immunofluorescence and immunohistochemical staining

Immunofluorescence staining (IF) was conducted as previously described by us [30]. Paraffin-embedded brain sections (4-μm thickness) were prepared as above-mentioned and antigen retrieval was performed with Citrate-EDTA Antigen Retrieval Solution (P0086, Beyotime, China) in a microwave oven lasting for 25 min. Subsequently, the sections were blocked with 5% goat serum(SL038, Solarbio life sciences, china) at room temperature for 30 min and then incubated overnight at 4 °C with the primary antibody as follows: Anti-HSP22 antibody (1:50, ab15515, Abcam), Anti-PGC1α antibody (1:200, ab54481, Abcam), Anti-Nrf1 antibody (1:100, AF5298, Affinity), Anti-Drp1 antibody (1:250, ab184247, Abcam), Anti-NeuN antibody (1:500, ab104224, Abcam). For immunofluorescent double-staining, primary antibodies were mixed and incubated under the same condition. Adjacently, the slices were washed with phosphate-buffered saline (PBS) and then incubated with corresponding secondary antibodies: Alexa Fluor 594 goat anti-mouse IgG, 1:400, Abcam, ab150116; Alexa Fluor 488 goat anti-rabbit IgG, 1:400, Abcam, ab150077; Goat Anti-Mouse IgG H&L (Alexa Fluor® 488), 1:400, Abcam, ab150113; Goat Anti-Rabbit IgG H&L (Alexa Fluor® 594),1:400, Abcam, ab150080) for 1 h at 37 °C. After washed with PBS, Hoechst 33342 (Sigma-Aldrich, USA) was employed to dye the nucleus for 15 min. Images were captured by a fluorescence microscope (Leica, DMI8, Germany).

Immunohistochemical staining was performed based on the commercial kit (SPN-9002, ZSGB-Bio, Beijing, China). Antigen repair was consistent with IF staining. After that, endogenous peroxidase activity was blocked employing 0.3% H_2O_2 for 10 min and then washed with PBS. After blocked by 5% goat serum for 15 min, slices were incubated overnight at 4 °C with the mouse monoclonal anti-8-OhdG antibody (1:500, ab62623, Abcam). Adjacently, sections were incubated with biotinylated goat anti-mouse IgG secondary antibody for 15 min and later with HRP-streptavidin reagent. Ultimately, immunoreactivity was visualized using 3,3-diaminobenzidine (DAB, Boster), followed by restaining with hematoxylin. Images were obtained via a light microscope (Leica, DM2500, Germany).

2.8. TUNEL staining and FJC staining

Neuronal apoptosis was detected with a Terminal deoxynucleotidyl transferase dUTP nick-end labeling (TUNEL) kit ((Roche Inc., Indianapolis, USA) in strict accordance with the instructions. Briefly, brain sections were incubated with TUNEL reaction mixture for 1 h at room temperature. After washed with PBS three times, the sections were stained with DAPI to show cell nuclei. Images were visualized and obtained under a light microscope system (Leica, DM2500, Germany). FJC staining was conducted to evaluate degenerated neurons with a commercial detection kit (Millipore, Darmstadt, Germany) as formerly elaborated [31]. The number of stained cells was analyzed by Image J software.

2.9. Measurement of mitochondrial DNA (mtDNA) content and ATP level

mtDNA copy number was measured by quantitative polymerase chain reaction (QT-PCR). The total DNA of the rat brain was isolated using DNeasy Blood and Tissue Kit (Qiagen, Valencia, CA) and mtDNA content was determined as mtDNA encoded mitochondrial 16s and normalized against the nuclear EEF1A1 using the $2^{-\triangle\triangle CT}$ method. The primers were synthesized by Takara Biomedical Technology as follows: mitochondrial 16s: Forward 5′-CCGCAAGGGAAAGATGAAAGAC-3′, Reverse 5′-TCGTTTGGTTTCGGGGTTTC-3’; nuclear EEF1A1: Forward 5′-GGATTGCCA CACGGCTCACATT-3′, Reverse 5′-GGTGGATAGTCTGAGAAGCTCTC-3’. Firefly luciferase-based ATP Assay Kit (S0026, Beyotime Biotechnology, Shanghai, China) was used for detecting ATP levels according to the instructions of the manufacturer.

2.10. Analysis of the morphology and amount of mitochondria

Briefly, after decapitated under deep anesthesia, the fresh cortex tissue blocks of the rat brain are isolated, with size no more than 1 mm^3. Adjacently, putting the tissue blocks in 2.5% glutaraldehyde (M8K7018, nacalai tesque, Japan) at 4 °C for 2–4 h. After washed with PBS, the tissue blocks were post-fixed with 1% OsO4 in 0.1 M PBS (pH 7.4) for 2 h at room temperature. Subsequently, after dehydration, infiltration and embedding, 60–80 nm ultrathin brain sections were obtained by Ultramicrotome (Leica UC7, Leica) and stained with uranyl acetate and lead citrate. Afterward, a transmission electron microscopy (HT7700, HITACHI) was employed to scrutinize the mitochondrial morphology and number of cortex tissues.

2.11. Measurement of ROS level

Dihydroethidium (DHE) staining was utilized to measure the ROS level of rat brains. Freshly prepared frozen brain sections (10 μm) were incubated with 2 μmol/L fluorescent dye dihydroethidium (DHE, Thermo Fisher Scientific, USA) at 37 °C for 30 min in a humidified chamber and protected from light. After cover-slipped, the images of DHE staining were obtained through a light microscope (Leica-DMi8, Microsystems, Germany), and the DHE-positive cells were counted by using ImageJ software (ImageJ, USA).

2.12. ELISA

The levels of brain oxidative damage indexes including 8-hydroxy-2-deoxyguanosine (8-OHdG), Protein Carbonyl (PCO) and Malondialdehyde (MDA) were respectively analyzed using the 8-OHdG assay kit, PCO assay kit and MDA assay kit, according to the manufacturer’s instructions. The levels of antioxidant factors superoxide dismutase (SOD) and glutathione peroxidase activity (GSHPx) were separately

determined by SOD assay Kit and GSHPx assay Kit in line with the manufacturer's instructions. All the kits are from Shanghai Enzyme-linked Biotechnology Co., Ltd. China.

2.13. Western blot

Western blot was conducted as formerly described [31]. First, protein extraction kits were used for the protein extraction of brain cortex tissues. Afterward, 30 μg of protein were separated by 7.5–15% SDS-PAGE gel electrophoresis and then transferred to PVDF membranes. Subsequently, PVDF membranes were blocked in 5% skim milk or BSA for 1 h at room temperature and incubated at 4 °C overnight with primary antibodies as follows: Anti-Hsp22 antibody (1:1000, ab15515, Abcam), Anti-AMPK antibody (1:1000, ab32047, Abcam), Anti-p-AMPK antibody (1:1000, AF3423, Affinity), Anti-PGC1α antibody (1:1000, ab54481, Abcam), Anti-Nrf1 antibody (1:1000, AF5298, Affinity), Anti-Drp1 antibody (1:1000, ab184247, Abcam), Anti-UCP2 antibody (1:1000, DF8626, Affinity), Anti-TFAM antibody (1:1000, DF6696, Affinity), Anti-Cytochrome C antibody (1:1000, 4280, Cell Signaling), Anti-COXⅣ antibody (1:1000, 4850, Cell Signaling), Anti- Cleaved caspase-3 antibody (1:1000, 4280S, Cell Signaling), Anti-Caspase-3 antibody (1:1000, AF6311, Affinity), Anti-Bax antibody (1:1000, 50599-2-Ig, Proteintech), Anti-Bcl-2 antibody (1:1000, 60178-1-Ig, Proteintech), Anti-β-actin antibody (1:1000, AF7018, Affinity). After rinsed with PBS, PVDF membranes were incubated with secondary antibodies (Goat Anti-Rabbit IgG(H + L), 1:10000, S0001, Affinity, USA, or Goat Anti-Mouse IgG(H + L), 1:10000, S0002, Affinity, USA) for 1 h at room temperature. Finally, the blots were visualized by the Affinity ECL kit and protein quantification was performed using ImageJ 1.5 software (National Institutes of Health, USA).

2.14. Statistical analysis

The data were presented as the mean ± standard deviation (SD) and all statistical analyses were performed using SPSS 19.0 software (SPSS, IBM, Armonk, NY, USA). Comparison between groups was determined by one-way analysis of variance (ANOVA) and followed by LSD test or Dunnett's T3 test for the two groups' comparison within the multiple groups. The statistical significance was determined when $P < 0.05$. Investigators were blinded to the identity of groups during the whole experiment.

3. Results

3.1. SAH model and time-course expression of Hsp22, p-AMPK/AMPK, and PGC1α after SAH

Representative photographs of the bottom of rat brains and HE staining from sham and 24 h after SAH are shown in Fig. 1A. The Mortality and excluded rat numbers per group, along with SAH grades are presented in Supplemental Fig. 2. The results of Western blot (WB) indicated that compared to the sham, the evident elevation of hsp22 started at 6 h post-SAH and peaked at 24 h, and then gradually declined until 72 h (Fig. 1C left). Simultaneously, the expressions of p-AMPK/AMPK and PGC1α have analogous tendencies as those of hsp22 (Fig. 1C middle and right). Additionally, double immunofluorescence (IF) staining exhibited that Hsp22 was localized in neurons (NeuN) of the cerebral cortex, and the number of hsp22-positive neurons was noticeably higher at 24 h post-SAH than the sham group (Fig. 1B).

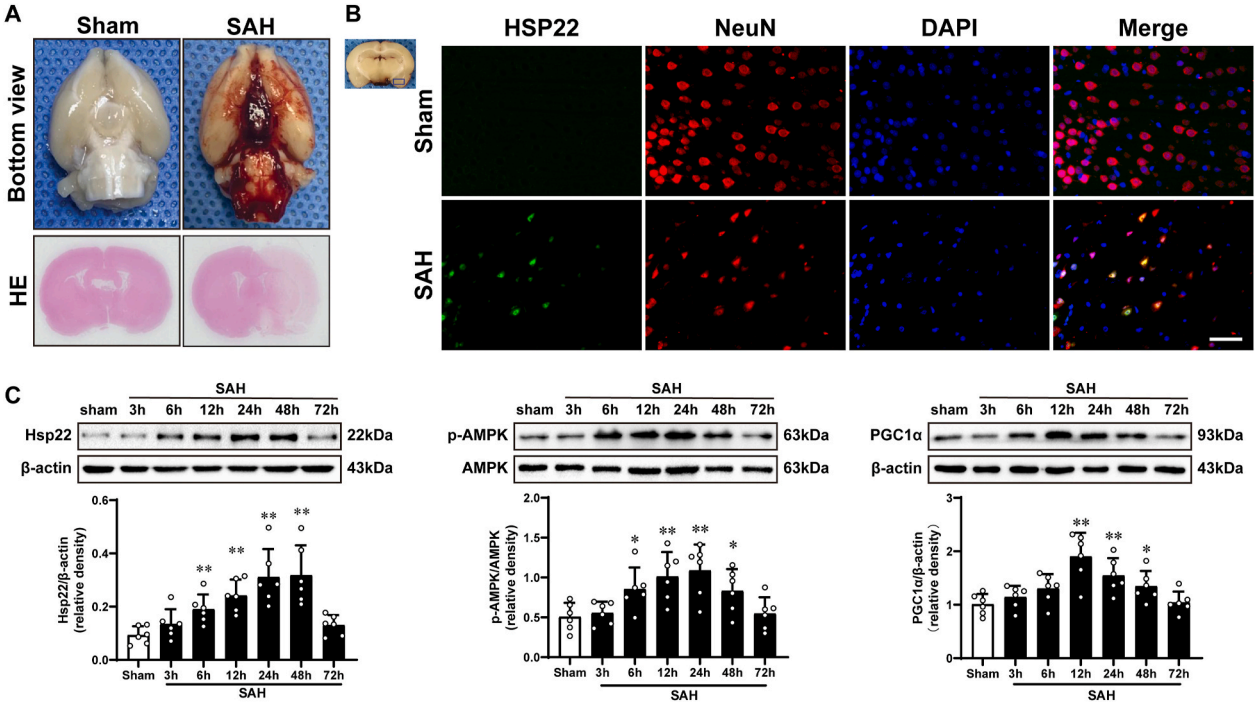

Fig. 1. Typical images of subarachnoid hemorrhage (SAH) model and expression alterations of Hsp22 (heat shock protein 22), p-AMPK/AMPK(adenosine 5'monophosphate-activated protein kinase) and PGC1α (peroxisome proliferative activated receptor γ (PPARγ) coactivator 1α) after SAH. (A) Representative photographs of the bottom of rat brains and HE staining from sham and 24 h after SAH. (B) Representative microphotographs of immunofluorescence staining for Hsp22 (green) co-localization on neurons (NeuN, red) after SAH. n = 2 per group. Scale bar = 50 μm. (C) Western blot assay and quantitative analysis of the temporal profiles of Hsp22, p-AMPK/AMPK and PGC1α expressions from the injured cortex at 3 h, 6 h, 12 h, 24 h, 48 h, and 72 h post-SAH. n = 6 per group. Bars represent mean ± SD. *$P < 0.05$, **$P < 0.01$ vs Sham group. . (For interpretation of the references to colour in this figure legend, the reader is referred to the Web version of this article.)

3.2. Hsp22 is intimately associated with the severity of EBI after SAH and mediates the variations of AMPK, PGC1α, NRF1, and DRP1 at 24 h post-SAH

We conducted the effectiveness of three diverse concentrations of hsp22 on aggravated neurological deficits (modified Garcia and beam balance tests), cerebral edema and apoptosis in response to SAH. The data showed that delivery of 10 μg/kg Hsp22 ameliorated the neurobehavioral scores, brain water content and apoptosis optimal among the hsp22-injected groups compared with the SAH + vehicle group (Supplemental Fig. 3). Therefore, hsp22 at 10 μg/kg was selected for subsequent experiments. Subsequently, the administration of hsp22 siRNA (The efficiency was confirmed by WB presented in Supplemental Fig. 4A) furtherly deteriorated the neurological deficits and brain edema in comparison to the SAH + scramble siRNA group (Fig. 2A). Meanwhile, FJC staining revealed that the degenerated neurons were notably increased post-SAH, and injection of hsp22 significantly decreased the dying neurons, while hsp22 siRNA further augmented the number of the SAH-induced neuronal degeneration (Fig. 2B). WB results demonstrated the expressions of p-AMPK, PGC1α, dynamin-related protein 1(DRP1), nuclear respiratory factor 1(NRF1) were remarkably increased in the SAH + vehicle group and scramble siRNA group when compared with the sham group. Meanwhile, Hsp22 treatment further enhanced the levels of p-AMPK, PGC1α, and NRF1, whereas inhibited the expression of DRP1 compared to the SAH + vehicle group. Conversely, the administration of hsp22 siRNA downregulated the expressions of p-AMPK, PGC1α, and NRF1, and concurrently upregulated the level of DRP1 (Fig. 2C). Moreover, in line with WB, similar changes of PGC1α, Drp1 and Nrf1 in neurons from diverse groups were also confirmed by IF (Fig. 2D).

3.3. Knockdown of PGC1α abolished the protective effects of hsp22 on the EBI and apoptotic cascades at 24 h after SAH

Compared with the control groups (SAH + Hsp22 group and SAH + Hsp22 scramble siRNA groups), knockdown of PGC1α by siRNA (The efficiency was authenticated by WB presented in Supplemental Fig. 4B) abated the beneficial effects of Hsp22 administration both on neurological scores (Beam balance and Modified Garcia) and brain water content (Fig. 3A). TUNEL staining showed that injection of hsp22

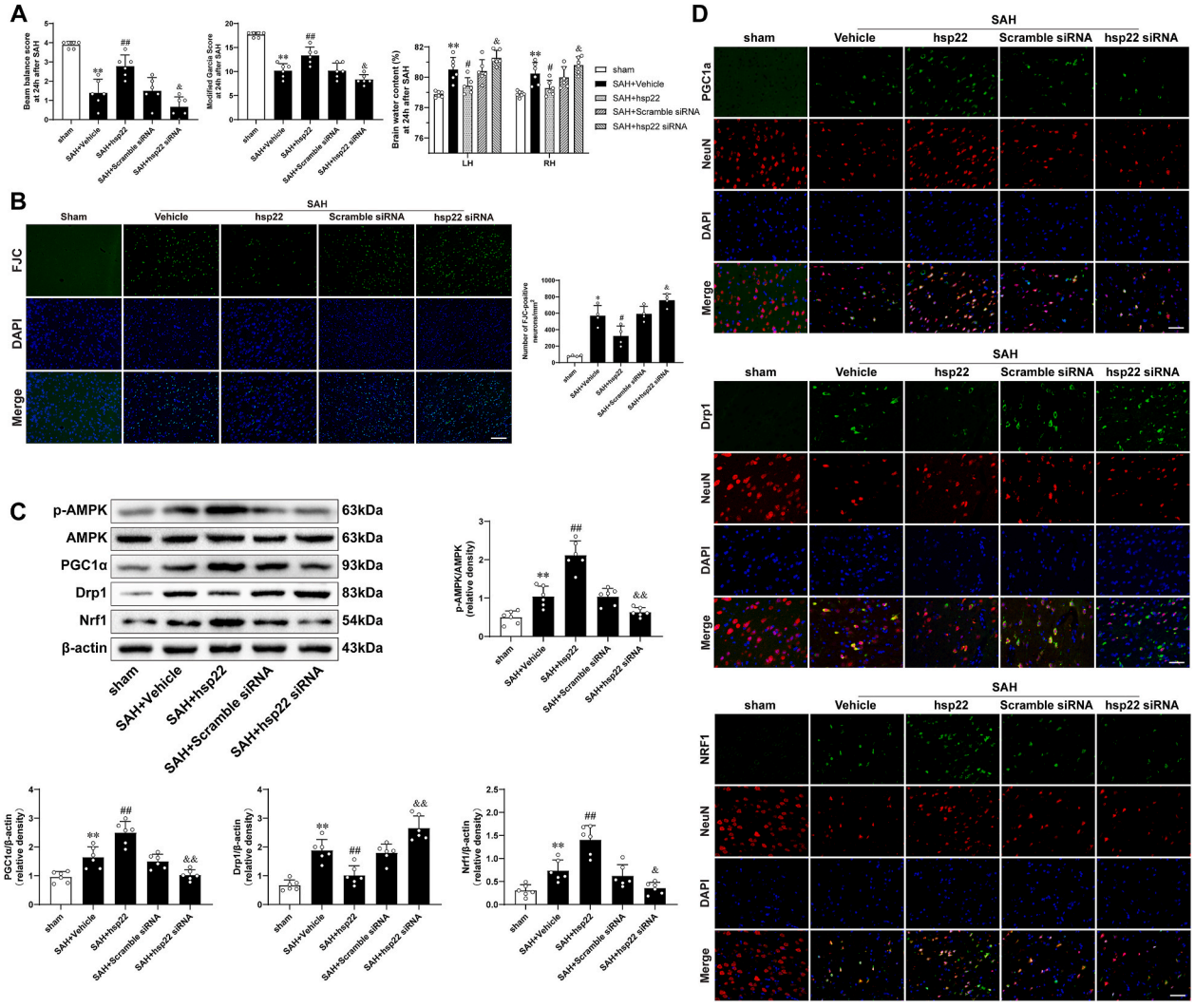

Fig. 2. Hsp22 is bound up with the severity of EBI post-SAH and mediates the alterations of p-AMPK/AMPK, PGC1α, DRP1, and NRF1. (A) Beam balance scores, Modified Garcia scores, and Brain water content at diverse groups. n = 6 per group. (B) FJC staining and quantitative analyses. n = 4 per group. Scale bar = 100 μm. (C) Representative Western blot images and quantitative analyses of p-AMPK/AMPK, PGC1α, NRF1, and DRP1. n = 6 per group. (D) Double immunofluorescence staining revealed the variations of PGC1α, NRF1, and DRP1(green) in the neuron (NeuN, red). n = 4 in each group. Scale bar = 50 μm. Bars represent mean ± SD. $^{*}P < 0.05$, $^{**}P < 0.01$ vs. sham group. $^{\#}P < 0.05$, $^{\#\#}P < 0.01$ vs. SAH + Vehicle group. $^{\&}P < 0.05$, $^{\&\&}P < 0.01$ vs. SAH + hsp22+scramble siRNA. (For interpretation of the references to colour in this figure legend, the reader is referred to the Web version of this article.)

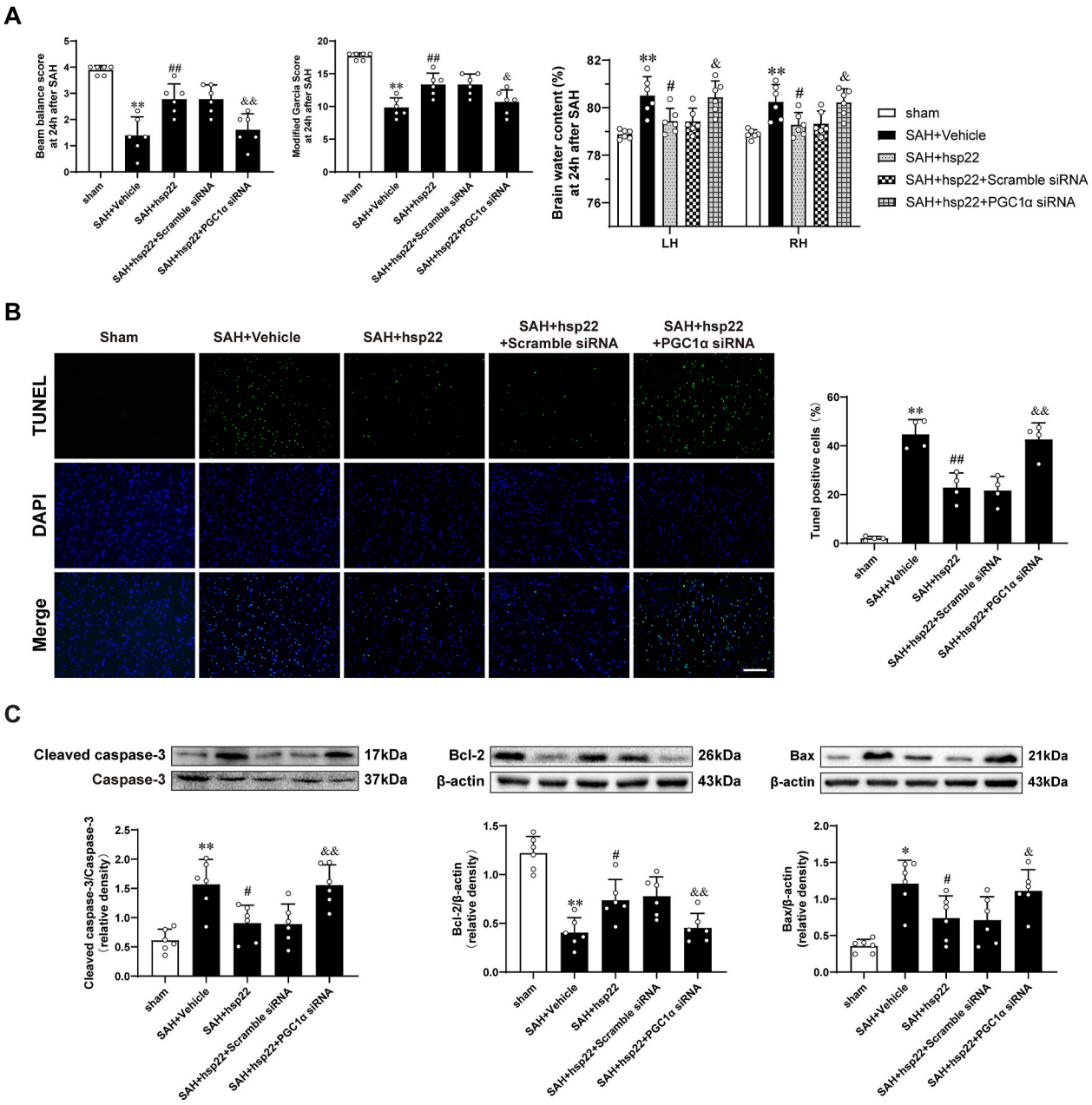

Fig. 3. Effects of PGC1α siRNA on hsp22-induced improvements in neurologic function and brain water content as well as apoptotic cascades after SAHBeam balance scores, Modified Garcia scores and Brain water content in different groups. n = 6 per group. (B) Typical photomicrographs of TUNEL staining and quantitative analyses in the indicated groups. n = 4. Scale bar = 100 μm. (C) Representative Western blot images and quantitative analyses of cleaved Caspase-3/Caspase-3, Bax and Bcl-2. n = 6 per group. Bars represent mean ± SD. $^{*}P < 0.05$, $^{**}P < 0.01$ vs. Sham group. $^{\#}P < 0.05$, $^{\#\#}P < 0.01$ vs. SAH + Vehicle group. $^{\&}P < 0.05$, $^{\&\&}P < 0.01$ vs. SAH + hsp22+scramble siRNA.

evidently inhibited the increase of the number of apoptotic cells post-SAH, whereas PGC1α siRNA reversed the number of Hsp22-mediated decrease of TUNEL positive cells (Fig. 3B). Additionally, compared with the sham group, expression of apoptosis-related proteins demonstrated Cleaved caspase-3 and Bax upregulated, while Bcl-2 downregulated remarkably in the SAH + vehicle group (Fig. 3C). On delivery of exogenous hsp22 eminently counteracted the abovementioned alterations. Conversely, PGC1α siRNA administration terminated the beneficial effects of hsp22 resulting in increased expression of Cleaved caspase-3 and Bax, along with a decrease in Bcl-2.

3.4. Knockdown of PGC1α blocked the beneficial properties of hsp22 on the regulation of disequilibrium of oxidation and anti-oxidation system at 24 h after SAH

SAH induced eminently oxidative damage, as evidenced by DHE staining and ELISA assays demonstrating increases in ROS, 8-OHdG, MDA, and PCO, and decreases in GSH-Px and SOD activities when compared with those of the sham + vehicle group (Fig. 4A, Fig. 4C and 4D). Contrarily, hsp22 administration partly counteracted the aforementioned variations, whereas injection of PGC1a siRNA compromised the favorable effects of hsp22 leading to increased levels of ROS, 8-OHdG, MDA, and PCO, and decreased activities of GSH-Px and SOD. In keeping with the results of ELISA, parallel alterations of 8-OHdG in different groups were also proved by immunohistochemical staining

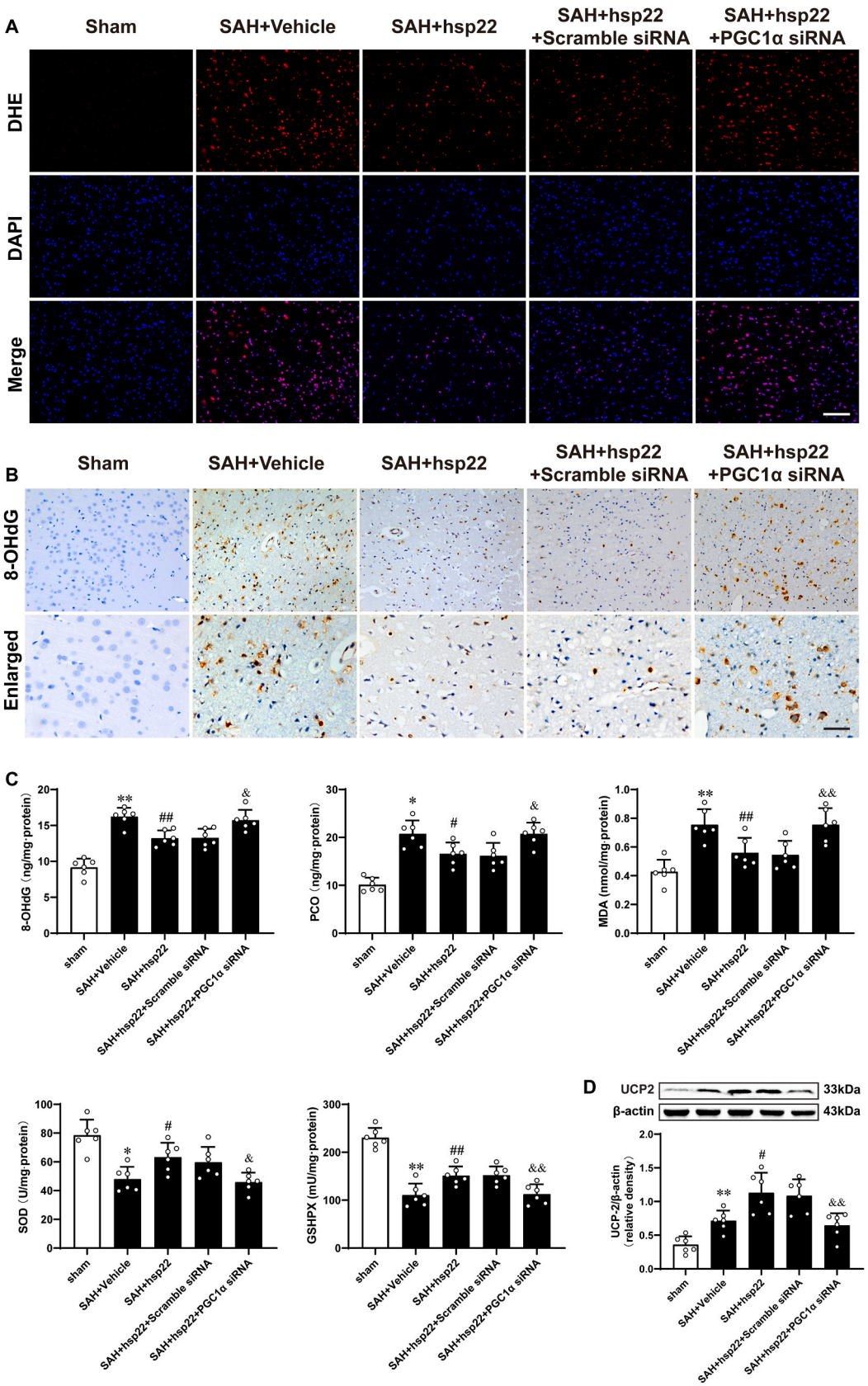

Fig. 4. Effects of PGC1α siRNA on hsp22-mediated protection against redox imbalance after SAH DHE staining in various groups. n = 4 per group. Scale bar = 100 μm (B) Immunohistochemical staining of 8-OHdG in the indicated groups. n = 4 per group. Scale bar = 100 μm (C) Elisa assay and quantitive analysis of different markers of oxidative damage (8-OHdG, MDA and PCO) and antioxidative indices (GSH-Px and SOD). n = 6 per group. (D) Representative Western blot images and quantitative analysis of UCP2. n = 6 per group. Bars represent mean ± SD. $^{*}P < 0.05$, $^{**}P < 0.01$ vs. Sham group. $^{\#}P < 0.05$, $^{\#\#}P < 0.01$ vs. SAH + Vehicle group. $^{\&}P < 0.05$, $^{\&\&}P < 0.01$ vs. SAH + hsp22+scramble siRNA.

(Fig. 4B). Furthermore, WB analysis indicated that the expression of uncoupling protein 2 (UCP2) augmented post-SAH, and injection of hsp22 further enhanced the level of UCP2, which was evidently abated by PGC1α siRNA (Fig. 4D).

3.5. Effects of PGC1α siRNA on hsp22-mediated protection of mitochondrial structure and function at 24 h after SAH

WB exhibited a significant increase in the expressions of TFAM, Nrf1 and Drp1 of the SAH + vehicle group when compared with the sham group (Fig. 5A). On administration of hsp22, the levels of TFAM, Nrf1 were further enhanced, whereas Drp1 was significantly lowered. Reciprocally, PGC1α siRNA remarkably reversed the above changes. In line with WB, IF staining demonstrated that hsp22-induced upregulation of Nrf1 in neurons was notably reversed by the delivery of PGC1α siRNA when compared with the SAH + hsp22+scramble siRNA group (Fig. 5B left). Meanwhile, treatment with PGC1α siRNA also counteracted exogenous hsp22-mediated downregulation of Drp1, boosting the expression of Drp1 in neurons (Fig. 5B right).

Besides, the data showed that the copy number of mtDNA and ATP content were significantly decreased after SAH when compared with the sham group, application of exogenous hsp22 eminently counteracted SAH-mediated decrease of them. Nevertheless, the silence of PGC1α abolished the effects of hsp22, leading to a decrease of mtDNA number and ATP content (Fig. 5C). Concomitantly, the WB assay indicated that SAH elicited notable translocation of Cytochrome c from mitochondria to the cytoplasm when compared with the sham group, which was blocked by exogenous hsp22. Interestingly, the administration of PGC1α siRNA abated the effects of hsp22, accelerating the translocation of cytochrome c (Fig. 5D). Moreover, the results of electron microscopy showed that after SAH, the mitochondria swelled, the mitochondrial cristae cracked and the number of mitochondria decreased. Administration of exogenous hsp22 mitigated the aforementioned variations, whereas combined delivery with PGC1α siRNA counteracted the improvement of hsp22 on the ultrastructure of mitochondria (Fig. 5E).

3.6. Hsp22 regulates PGC1α via an AMPK signaling pathway

Compared to the SAH + hsp22 group, suppression of AMPK with dorsomorphin reversed the protective roles of exogenous hsp22 on neurological deficits and brain edema (Fig. 6A) as well as cell apoptosis (as evidenced by TUNEL staining, Fig. 6B). Additionally, administration of dorsomorphin also resulted in a significant decrease of hsp22 mediated-upregulation of p-AMPK/AMPK, PGC1a, Nrf1, mitochondrial transcription factor A(TFAM), UCP2, Bcl-2, and cytosolic cytochrome *c*, and *a* notable increase of hsp22 mediated-downregulation of Drp1, Cleaved caspase-3/Caspase-3, Bax and mitochondrial cytochrome c when compared with the SAH + hsp22 group (Fig. 6D). Furthermore, in keeping with the results of Wb, parallel variations of PGC1α in neurons from various groups were also confirmed by IF staining (Fig. 6C).

4. Discussion

In the present study, we found that the expressions of Hsp22, p-AMPK/AMPK and PGC1α were notably upregulated at 24 h after SAH and eminently associated with the severity of EBI. Exogenous hsp22 increased the expressions of p-AMPK and PGC1α, ameliorated TFAM/Nrf1-mediated mitochondrial biogenesis, and suppressed Drp1-triggered mitochondrial apoptosis, thus alleviating the neurological deficits and brain edema, whereas knockdown of hsp22 reversed the above protective effects. Additionally, silencing PGC1α abolished the favorable roles of hsp22 on the improvement of EBI, regulation of disequilibrium of oxidation and anti-oxidation system, and modulation of mitochondrial biogenesis, fission, as well as mitochondria-dependent apoptosis. Importantly, inhibition of AMPK with dorsomorphin resulted in a significant decrease of hsp22 mediated-upregulation of PGC1α, TFAM, Nrf1, UCP2, and BCL2, and an increase of hsp22 mediated-downregulation of cleaved caspase-3 and Bax at 24 h after SAH. Taken together, our findings indicate that hsp22 conveys neuroprotection via attenuation of mitochondrial damage by modulating TFAM/Nrf1-dependent mitochondrial biogenesis and Drp1-mediated mitochondrial apoptosis cascade after SAH, at least in part through the AMPK-PGC1α signaling pathway.

HSP22, a small heat shock protein, has recently been reported to have beneficial properties against oxidative stress [16,18], mitochondrial dysfunction [20], endothelial injury [19], aging [14] and apoptosis [32]. Concretely, an in vitro study showed that overexpression of hsp22 markedly restrained H_2O_2-induced hippocampal neuronal cell death by modulation of the mitochondrial-related apoptosis pathway [20]. Moreover, in a rat middle cerebral artery occlusion/reperfusion model, lentivirus-mediated hsp22 over-expression potently alleviated infarct volume and ameliorated neurobehavioral outcomes and cerebral edema [17]. The current study demonstrated that extrinsic hsp22 noticeably repressed the SAH-elicited oxidative cascade reactions, ameliorated neuronal degeneration and apoptosis, alleviated neurological deficits as well as brain edema. Reciprocally, knockdown of hsp22 remarkably reversed the above processes, which was partly in accord with the prior reports of cerebral ischemia-reperfusion injury [32] and cardiac overload [21].

It is wide-accepted that mitochondria play a decisive role in the pathological processes of ATP depletion, oxidative stress, and cell apoptosis. The homeostasis of mitochondria is controlled by differential interactions of mitochondrial biogenesis, fusion, and fission-related proteins [33]. Normal mitochondrial fission/fusion maintains a healthy mitochondrial network, while aberrant mitochondrial fission caused by DRP1 induces ROS overproduction, and triggers the caspase-3-dependent death pathway by the release of cytochrome c into the cytoplasm [12,13] in various disease models. As a remedy for mitochondrial dysfunction, restraint of Drp1 activation was shown to reverse the above alterations, restore mitochondrial function and morphology, ultimately attenuating the early brain injury after SAH [34]. Astonishingly, in a hyperglycemia-induced endothelial injury model, hsp22 was reported to modulate the balance of mitochondrial fusion and fission by inhibiting the upregulation of Drp1 and its phosphorylation level [20]. Our data showed that exogenous hsp22 significantly suppressed the Drp1 expression and silencing hsp22 reversed the trend, implying a negative regulation that exists between hsp22 and Drp1, however, the exact signaling cascades mediating the possible hsp22-Drp1 crosstalk and improvement of mitochondrial dysfunction after SAH remains obscure.

PGC1α, a recognized transcription coactivator, interferes with the expression of drp1 by directly binding to its transcription promoter, as evidenced by Chromatin immunoprecipitation [29], thus preventing Drp1-mediated mitochondrial fission and apoptosis [11]. In the present study, we found that enhancement of PGC1α by hsp22 administration suppressed drp1 expression as expected, while PGC1α siRNA blocked the down-regulation effect of hsp22 on drp1 expression. Hence, we boldly speculated that hsp22 may inhibit drp1-mediated mitochondrial fission by upregulating PGC1α. Also, PGC1α siRNA reversed the blocking effect of hsp22 on excessive mitochondrial division, leading to the release of cytochrome c to the cytoplasm, and activation of the caspase-3-related apoptosis cascades, which further confirmed our hypothesis. Besides, PGC1α has multiple implications on mitochondria, well beyond its regulation on drp1-mediated mitochondrial fission, including activation of mitochondrial biogenesis [35] and amelioration of oxidative stress [36].

Mitochondrial transcription factor A(TFAM), a principal mitochondrial gene-regulator, is essential for mitochondrial DNA (mtDNA) maintenance along with mitochondrial dynamics, contributing to ROS scavenging and cell survival [37,38]. As an effector of nucleo-mitochondrial interactions, the nuclear respiratory factor 1 (NRF-1) was also stated to be eminently pertinent to the biogenesis of

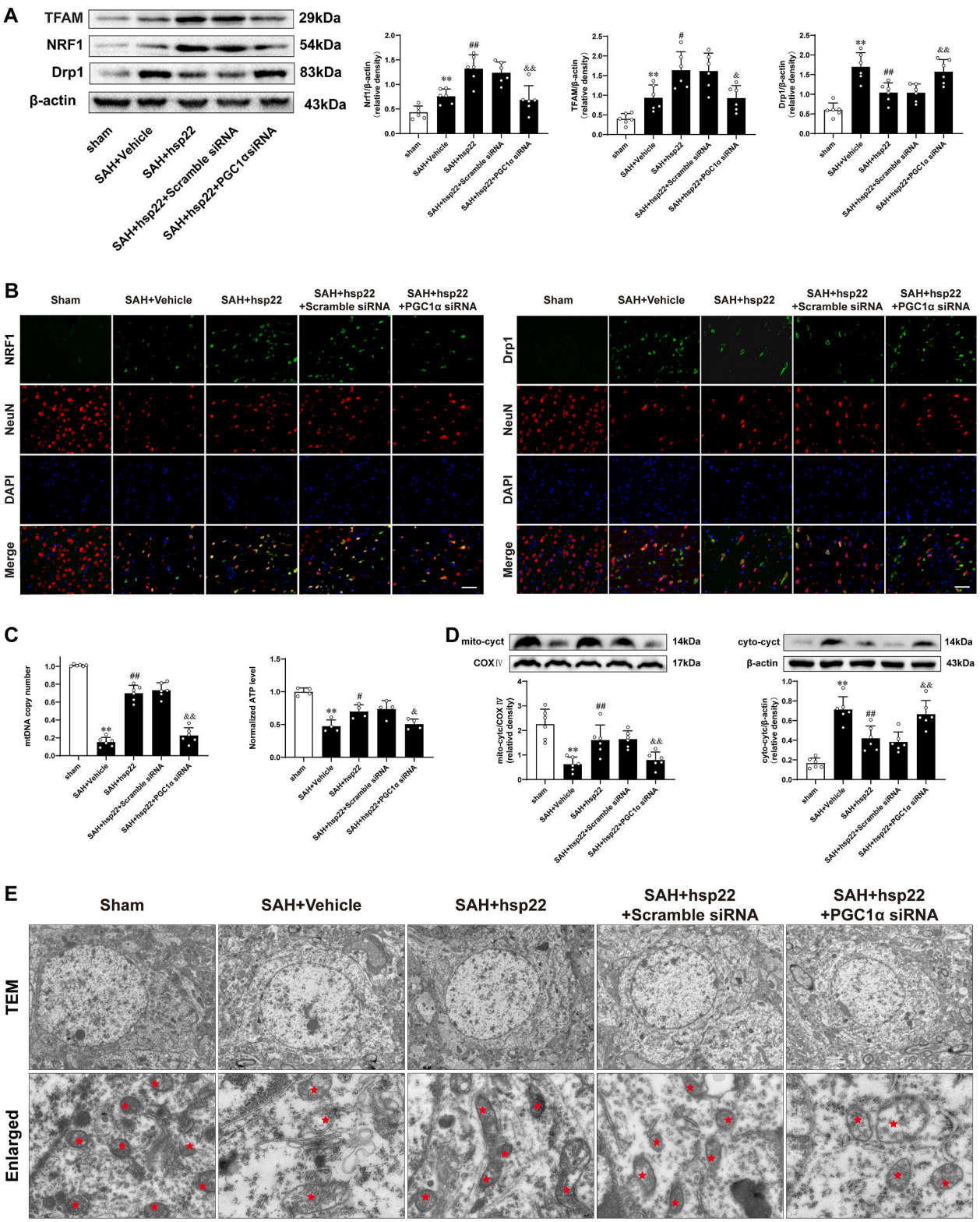

Fig. 5. Effects of PGC1α siRNA on hsp22-mediated protection of mitochondrial structure and function following SAH Representative Western blot images and quantitative analyses of TFAM, Nrf1 and Drp1 of different groups. n = 6 per group. (B) Double immunofluorescence staining for Nrf1 and Drp1 (green) in the neuron (NeuN, red) in diverse groups. n = 4 per group. Scale bar = 50 μm. (C) mtDNA copy number and ATP content in the indicated groups. n = 6 per group. (D) Representative Western blot images and quantitative analyses of mitochondrial cytochrome c and cytoplasmic cytochrome c from five groups. n = 6 per group. (E) Transmission electron microscope (TEM) of cortical neurons. n = 4 per group. The red star stands for mitochondria. Bars represent mean ± SD. $^{*}P < 0.05$, $^{**}P < 0.01$ vs. Sham group. $^{\#}P < 0.05$, $^{\#\#}P < 0.01$ vs. SAH + Vehicle group. $^{\&}P < 0.05$, $^{\&\&}P < 0.01$ vs. SAH + hsp22+scramble siRNA. (For interpretation of the references to colour in this figure legend, the reader is referred to the Web version of this article.)

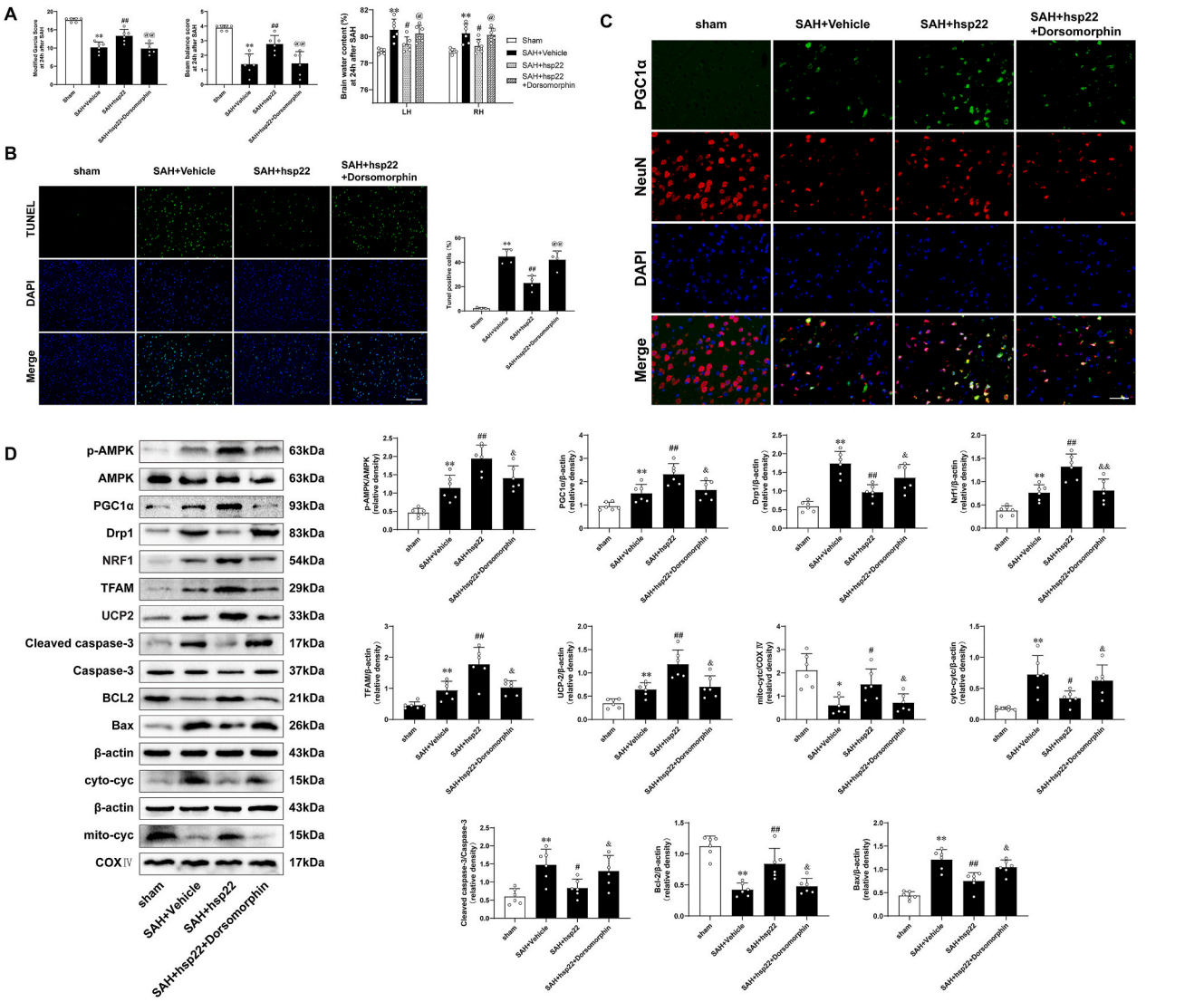

Fig. 6. Hsp22 regulates PGC1α via AMPK signaling pathway in rats after SAH Beam balance scores, Modified Garcia scores and Brainwater content in various groups. n = 6 per group. (B) Representative photomicrographs of TUNEL staining and quantitative analyses in the indicated groups. n = 4 per group. Scale bar = 100 μm. (C) Typical photomicrographs showing double immunofluorescence staining of PGC1α (green) and NeuN (red) in diverse experimental groups. n = 4 per group. Scale bar = 50 μm. (D) Western blot images and quantitative analyses of p-AMPK/AMPK, PGC1α, Drp1, Nrf1, TFAM, UCP2, Cleaved caspase-3/Caspase-3, Bcl2, Bax, Cytosolic and mitochondrial cytochrome c. n = 6 per group. Bars represent mean ± SD. $^{**}P < 0.01$, $^{*}P < 0.05$ vs. Sham group. $^{\#\#}P < 0.01$, $^{\#}P < 0.05$ vs. SAH + Vehicle group. $^{\&\&}P < 0.01$, $^{\&}P < 0.05$ vs. SAH + hsp22+scramble siRNA. (For interpretation of the references to colour in this figure legend, the reader is referred to the Web version of this article.)

mitochondria [39]. More importantly, potent evidence confirmed that PGC1α is engaged in the maintenance of mtDNA transcription and replication by transcriptional control of Nrf1 and TFAM [40]. Furthermore, it is thought that mtDNA contributes to mitochondrial content and ATP production by encoding essential components of oxidative phosphorylation [41]. Surprisingly, recent studies have shown that PGC1α upregulation dramatically promoted the recovery of neurological function in neurodegenerative diseases and stroke through augmenting the replication of mtDNA, ATP production, and alleviating oxidative damage [42,43]. However, it is still scarce whether mitochondrial biogenesis participates in the pathological process of EBI after SAH. The present results identified that PGC1α was increased in cortex neurons post-SAH and upregulation of PGC1α by exogenous hsp22 enhanced mtDNA copy number, mitochondrial content and ATP level, accompanied with elevation of TFAM and Nrf1. In contrast, silencing PGC1α blocked the induction of hsp22 on the aforesaid indexes, potently indicating that the impacts of hsp22 on mitochondrial biogenesis may rely on PGC1α, which was firstly mentioned in the literature.

Uncoupling protein 2 (UCP2), a mitochondrial inner membrane anion-carrier protein transcriptionally regulated by PGC1α, acts an extremely crucial role in oxidative stress and apoptosis [44,45]. Upregulation of UCP2 conveyed neuroprotective effects, in SAH [7], cerebral ischemia [46,47], hypoxic-ischemic encephalopathy [48] and aging [49], which are mainly attributed to ROS reduction. Our data exhibited that SAH-induced increase of UCP2 and decrease of antioxidant markers SOD and GSHPx activities were markedly reversed, while SAH-triggered ROS production and augmentation of various indicators of oxidative damage (including 8-OHdG, MDA and PCO) were remarkably restrained when treatment with exogenous hsp22. Conversely, PGC1α knockdown abolished the antioxidative roles of hsp22, jointly reminding us that the influence of hsp22 on SAH-sparked redox imbalance may also hinge on PGC1α. Nonetheless, it is still undefined how Hsp22 regulates PGC1α, ameliorates mitochondrial dysfunction and concomitantly mitigates oxidative stress.

Adenosine 5'monophosphate-activated protein kinase (AMPK) serves as an endocellular energy sensor. Previous findings have

indicated that hsp22 directly binds to AMPK and promotes its nuclear translocation and phosphorylation at Thr172, which results in a stimulation of survival mechanisms [27]. Additionally, activators and suppressants of AMPK have been employed to verify that AMPK exerts a protective role in mitochondrial dynamics imbalance and oxidative stress-mediated myocardium [50–52], brain [28,53,54] and liver injury [25]. But, it is still little known whether hsp22-induced upregulation of p-AMPK is answerable for its protective properties on mitochondrial dysfunction in SAH. Presently, we observed that exogenous hsp22 obviously augmented the AMPK phosphorylation at Thr172, whereas dorsomorphin evidently counteracted hsp22-mediated protection against EBI after SAH by worsening neurological impairment and brain edema, aggravating mitochondrial fission and the outbreak of oxidative stress, and suppressing mitochondrial biogenesis and apoptotic cascades. More fundamentally, it is well established that activating AMPK by phosphorylation at Thr172 site upregulates PGC1α in skeletal muscle [55] and cardiovascular system [56], as well as brain [57]. Accordingly, it's logical to conjecture that hsp22 may alter PGC1α activity by enhancing AMPK phosphorylation at the same site. Interestingly, inhibition of AMPK with dorsomorphin also abrogated the influence of hsp22 on the PGC1α-related signaling molecules, furtherly hinting that the regulated effect of hsp22 on PGC1α and mitochondrial function may be mainly ascribed to the activation of AMPK after SAH induction.

Although the present study verified the value of Hsp22 in a novel mitochondria-relevant mechanism that mediated neuroprotection via activation of the AMPK- PGC1α signaling pathway in the SAH model, some limitations could not be ignored. First, it seems to be better to use a transgenic mouse model to exclude many background differences. Second, our experiments were particularly focused on the regulatory effects of hsp22 on mitochondrial fission and biogenesis and redox imbalance, without the exploration of its capability in autophagy-regulation and inflammation in the SAH model, which warrants further investigation.

In conclusion, the current study shows that hsp22 is upregulated at 24 h after SAH and exerts neuroprotection via amelioration of mitochondrial damage by triggering TFAM-induced mitochondrial biogenesis and extinguishing Drp1-mediated mitochondrial apoptosis cascade in an AMPK-PGC1α dependent manner. These findings identify hsp22-modulated mitochondrial biogenesis and fission as potential targets for salvaging EBI after SAH.

Declaration of competing interest

The authors report no conflicts of interest in this work.

Acknowledgments

This work was supported by the National Key Research and Development Project (Grant number: 2016YFC1300800) and the National Natural Science Foundation Project (Grant number: 81974178).

Appendix A. Supplementary data

Supplementary data to this article can be found online at https://doi.org/10.1016/j.redox.2021.101856.

References

[1] H. Suzuki, Y. Hasegawa, W. Chen, K. Kanamaru, J.H. Zhang, Recombinant osteopontin in cerebral vasospasm after subarachnoid hemorrhage, Ann. Neurol. 68 (5) (2010) 650–660.
[2] Z. Xin, K. Tamrakar, Y. Zhi-Qiang, D. Chuan-Zhi, et al., High wall shear stress beyond a certain range in the parent artery could predict the risk of anterior communicating artery aneurysm rupture at follow-up, J. Neurosurg. 131 (2018) 868–875.
[3] R.L. Macdonald, T.A. Schweizer, Spontaneous subarachnoid haemorrhage, Lancet 389 (10069) (2017) 655–666.
[4] W.J. Cahill, J.H. Calvert, J.H. Zhang, Mechanisms of early brain injury after subarachnoid hemorrhage, J. Cerebr. Blood Flow Metabol. 26 (11) (2006) 1341–1353.
[5] M.P. Mattson, M. Gleichmann, A. Cheng, Mitochondria in neuroplasticity and neurological disorders, Neuron 60 (5) (2008) 748–766.
[6] T. Zhang, P. Wu, E. Budbazar, Q. Zhu, C. Sun, J. Mo, J. Peng, V. Gospodarev, J. Tang, H. Shi, others, Mitophagy reduces oxidative stress via Keap1 (Kelch-Like epichlorohydrin-associated protein 1)/nrf2 (nuclear factor-E2-related factor 2)/PHB2 (prohibitin 2) pathway after subarachnoid hemorrhage in rats, Stroke 50 (4) (2019) 978–988.
[7] J. Mo, B. Enkhjargal, Z.D. Travis, K. Zhou, P. Wu, G. Zhang, Q. Zhu, T. Zhang, J. Peng, W. Xu, others, AVE 0991 attenuates oxidative stress and neuronal apoptosis via Mas/PKA/CREB/UCP-2 pathway after subarachnoid hemorrhage in rats, Redox Biology 20 (2019) 75–86.
[8] J.L. Franklin, Redox regulation of the intrinsic pathway in neuronal apoptosis, Antioxidants Redox Signal. 14 (8) (2011) 1437–1448.
[9] S.-D. Chen, D.-I. Yang, T.-K. Lin, F.-Z. Shaw, C.-W. Liou, Y.-C. Chuang, Roles of oxidative stress, apoptosis, PGC-1α and mitochondrial biogenesis in cerebral ischemia, Int. J. Mol. Sci. 12 (10) (2011) 7199–7215.
[10] W. Yin, A.P. Signore, M. Iwai, G. Cao, Y. Gao, J. Chen, Rapidly increased neuronal mitochondrial biogenesis after hypoxic-ischemic brain injury, Stroke 39 (11) (2008) 3057–3063.
[11] Q. Wang, M. Zhang, G. Torres, S. Wu, C. Ouyang, Z. Xie, M. Zou, Metformin suppresses diabetes-accelerated atherosclerosis via the inhibition of drp1-mediated mitochondrial fission, Diabetes 66 (1) (2017) 193–205.
[12] P. Clerc, S. Ge, H. Hwang, J. Waddell, B. Roelofs, M. Karbowski, H. Sesaki, B. Polster, Drp1 is dispensable for apoptotic cytochrome c release in primed MCF10A and fibroblast cells but affects Bcl-2 antagonist-induced respiratory changes, Br. J. Pharmacol. 171 (8) (2014) 1988–1999.
[13] J. Du, P. Hang, Y. Pan, B. Feng, Y. Zheng, T. Chen, L. Zhao, Z. Du, Inhibition of miR-23a attenuates doxorubicin-induced mitochondria-dependent cardiomyocyte apoptosis by targeting the PGC-1α/Drp1 pathway, Toxicol. Appl. Pharmacol. 369 (2019) 73–81.
[14] G. Morrow, S. Battistini, P. Zhang, R.M. Tanguay, Decreased lifespan in the absence of expression of the mitochondrial small heat shock protein Hsp22 in Drosophila, J. Biol. Chem. 279 (42) (2004) 43382–43385.
[15] G. Morrow, M. Samson, S. Michaud, R.M. Tanguay, Overexpression of the small mitochondrial Hsp22 extends Drosophila life span and increases resistance to oxidative stress, Faseb. J. 18 (3) (2004) 598–599.
[16] W. Wu, L. Lai, M. Xie, H. Qiu, Insights of heat shock protein 22 in the cardiac protection against ischemic oxidative stress, Redox Biology 34 (2020) 101555.
[17] F. Li, B. Yang, T. Li, X. Gong, F. Zhou, Z. Hu, HSPB8 over-expression prevents disruption of blood-brain barrier by promoting autophagic flux after cerebral ischemia/reperfusion injury, J. Neurochem. 148 (1) (2019) 97–113.
[18] G. Morrow, M. Le Pécheur, R.M. Tanguay, Drosophila melanogaster mitochondrial Hsp22: a role in resistance to oxidative stress, aging and the mitochondrial unfolding protein response, Biogerontology 17 (1) (2015) 61–70.
[19] L. Yu, Q. Liang, W. Zhang, M. Liao, M. Wen, B. Zhan, H. Bao, X. Cheng, HSP22 suppresses diabetes-induced endothelial injury by inhibiting mitochondrial reactive oxygen species formation, Redox Biology 21 (2019) 101095.
[20] H.S. Jo, D.W. Kim, M.J. Shin, S.B. Cho, J.H. Park, C.H. Lee, E.J. Yeo, Y.J. Choi, H. J. Yeo, E.J. Sohn, others, Tat-HSP22 inhibits oxidative stress-induced hippocampal neuronal cell death by regulation of the mitochondrial pathway, Mol. Brain 10 (1) (2017).
[21] H. Qiu, P. Lizano, L. Laure, X. Sui, E. Rashed, J.Y. Park, C. Hong, S. Gao, E. Holle, D. Morin, others, H11 kinase/heat shock protein 22 deletion impairs both nuclear and mitochondrial functions of STAT3 and accelerates the transition into heart failure on cardiac overload, Circulation 124 (4) (2011) 406–415.
[22] Y. Zhang, Y. Wang, J. Xu, F. Tian, S. Hu, Y. Chen, Z. Fu, Melatonin attenuates myocardial ischemia-reperfusion injury via improving mitochondrial fusion/mitophagy and activating the AMPK-OPA1 signaling pathways, J. Pineal Res. 66 (2) (2019), e12542.
[23] H. Zhou, S. Wang, P. Zhu, S. Hu, Y. Chen, J. Ren, Empagliflozin rescues diabetic myocardial microvascular injury via AMPK-mediated inhibition of mitochondrial fission, Redox Biology 15 (2018) 335–346.
[24] Y. Ren, H.-M. Shen, Critical role of AMPK in redox regulation under glucose starvation, Redox Biology 25 (2019) 101154.
[25] S.M. Park, S.W. Kim, E.H. Jung, H.L. Ko, C.K. Im, J.R. Lee, S.H. Byun, S.K. Ku, S. C. Kim, C.A. Park, others, Sipjeondaebo-tang alleviates oxidative stress-mediated liver injury through activation of the CaMKK2-AMPK signaling pathway, Evid. base Compl. Alternative Med. 2018 (2018) 1–13.
[26] S. Jiang, T. Li, T. Ji, W. Yi, Z. Yang, S. Wang, Y. Yang, C. Gu, AMPK: potential therapeutic target for ischemic stroke, Theranostics 8 (16) (2018) 4535–4551.
[27] C. Depre, L. Wang, X. Sui, H. Qiu, C. Hong, N. Hedhli, A. Ginion, A. Shah, M. Pelat, L. Bertrand, others, H11 kinase prevents myocardial infarction by preemptive preconditioning of the heart, Circ. Res. 98 (2) (2006) 280–288.
[28] W. Xu, T. Li, L. Gao, J. Zheng, J. Yan, J. Zhang, A. Shao, Apelin-13/APJ system attenuates early brain injury via suppression of endoplasmic reticulum stress-associated TXNIP/NLRP3 inflammasome activation and oxidative stress in a AMPK-dependent manner after subarachnoid hemorrhage in rats, J. Neuroinflammation 16 (1) (2019).
[29] M. Ding, N. Feng, D. Tang, J. Feng, Z. Li, M. Jia, Z. Liu, X. Gu, Y. Wang, F. Fu, others, Melatonin prevents Drp1-mediated mitochondrial fission in diabetic hearts through SIRT1-PGC1α pathway, J. Pineal Res. 65 (2) (2018), e12491.
[30] W. Liu, R. Li, J. Yin, S. Guo, Y. Chen, H. Fan, G. Li, Z. Li, X. Li, X. Zhang, others, Mesenchymal stem cells alleviate the early brain injury of subarachnoid

hemorrhage partly by suppression of Notch1-dependent neuroinflammation: involvement of Botch, J. Neuroinflammation 16 (1) (2019) 8.
[31] R. Li, W. Liu, J. Yin, Y. Chen, S. Guo, H. Fan, X. Li, X. Zhang, X. He, C. Duan, TSG-6 attenuates inflammation-induced brain injury via modulation of microglial polarization in SAH rats through the SOCS3/STAT3 pathway, J. Neuroinflammation 15 (1) (2018).
[32] F. Li, J. Tan, F. Zhou, Z. Hu, B. Yang, Heat shock protein B8 (HSPB8) reduces oxygen-glucose deprivation/reperfusion injury via the induction of mitophagy, Cell. Physiol. Biochem. 48 (4) (2018) 1492–1504.
[33] J. Meyer, T. Leuthner, A. Luz, Mitochondrial fusion, fission, and mitochondrial toxicity, Toxicology 391 (2017) 42–53.
[34] P. Wu, Y. Li, S. Zhu, C. Wang, J. Dai, G. Zhang, B. Zheng, S. Xu, L. Wang, T. Zhang, others, Mdivi-1 alleviates early brain injury after experimental subarachnoid hemorrhage in rats, possibly via inhibition of drp1-activated mitochondrial fission and oxidative stress, Neurochem. Res. 42 (5) (2017) 1449–1458.
[35] S.E. Fanibunda, S. Deb, B. Maniyadath, P. Tiwari, U. Ghai, S. Gupta, D. Figueiredo, N. Weisstaub, J.A. Gingrich, A.D.B. Vaidya, others, Serotonin regulates mitochondrial biogenesis and function in rodent cortical neurons via the 5-HT2A receptor and SIRT1–PGC-1α axis, Proc. Natl. Acad. Sci. Unit. States Am. 116 (22) (2019) 11028–11037.
[36] M.T. Tran, Z.K. Zsengeller, A.H. Berg, E.V. Khankin, M.K. Bhasin, W. Kim, C. B. Clish, I.E. Stillman, S.A. Karumanchi, E.P. Rhee, others, PGC1α drives NAD biosynthesis linking oxidative metabolism to renal protection, Nature 531 (7595) (2016) 528–532.
[37] D. Kang, S. Kim, N. Hamasaki, Mitochondrial transcription factor A (TFAM): roles in maintenance of mtDNA and cellular functions, Mitochondrion 7 (2007) 39–44.
[38] M. Ekstrand, M. Falkenberg, A. Rantanen, C. Park, M. Gaspari, K. Hultenby, P. Rustin, C. Gustafsson, N. Larsson, Mitochondrial transcription factor A regulates mtDNA copy number in mammals, Hum. Mol. Genet. 13 (9) (2004) 935–944.
[39] D. Hickson-Bick, C. Jones, L. Buja, Stimulation of mitochondrial biogenesis and autophagy by lipopolysaccharide in the neonatal rat cardiomyocyte protects against programmed cell death, J. Mol. Cell. Cardiol. 44 (2) (2008) 411–418.
[40] J. Santos, S. Tewari, A. Goldberg, R. Kowluru, Mitochondrial biogenesis and the development of diabetic retinopathy, Free Radic. Biol. Med. 51 (10) (2011) 1849–1860.
[41] G.H. Kunkel, P. Chaturvedi, S.C. Tyagi, Mitochondrial pathways to cardiac recovery: TFAM, Heart Fail. Rev. 21 (5) (2016) 499–517.
[42] S.D. Chen, T.K. Lin, D.I. Yang, S.Y. Lee, F.Z. Shaw, C.W. Liou, Y.C. Chuang, Protective effects of peroxisome proliferator-activated receptors gamma coactivator-1alpha against neuronal cell death in the hippocampal CA1 subfield after transient global ischemia, J. Neurosci. Res. 88 (3) (2010) 605–613.
[43] P. Wareski, A. Vaarmann, V. Choubey, D. Safiulina, J. Liiv, M. Kuum, A. Kaasik, PGC-1{alpha} and PGC-1{beta} regulate mitochondrial density in neurons, J. Biol. Chem. 284 (32) (2009) 21379–21385.
[44] B. Han, W. Jiang, H. Liu, J. Wang, K. Zheng, P. Cui, Y. Feng, C. Dang, Y. Bu, Q. Wang, others, Upregulation of neuronal PGC-1α ameliorates cognitive impairment induced by chronic cerebral hypoperfusion, Theranostics 10 (6) (2020) 2832–2848.
[45] H. Bhagani, S. Nasser, A. Dakroub, A. El-Yazbi, A. Eid, F. Kobeissy, G. Pintus, A. Eid, The mitochondria: a target of polyphenols in the treatment of diabetic cardiomyopathy, Int. J. Mol. Sci. 21 (14) (2020).
[46] J. Su, J. Liu, X. Yan, Y. Zhang, J. Zhang, L. Zhang, L. Sun, Cytoprotective effect of the UCP2-SIRT3 signaling pathway by decreasing mitochondrial oxidative stress on cerebral ischemia-reperfusion injury, Int. J. Mol. Sci. 18 (7) (2017).
[47] B. Zhao, L. Sun, X. Jiang, Y. Zhang, J. Kang, H. Meng, H. Li, J. Su, Genipin protects against cerebral ischemia-reperfusion injury by regulating the UCP2-SIRT3 signaling pathway, Eur. J. Pharmacol. 845 (2019) 56–64.
[48] J. Huang, W. Liu, D. Doycheva, M. Gamdzyk, W. Lu, J. Tang, J. Zhang, Ghrelin attenuates oxidative stress and neuronal apoptosis via GHSR-1α/AMPK/Sirt1/PGC-1α/UCP2 pathway in a rat model of neonatal HIE, Free Radic. Biol. Med. 141 (2019) 322–337.
[49] R. Crescenzo, M. Spagnuolo, R. Cancelliere, L. Iannotta, A. Mazzoli, C. Gatto, S. Iossa, L. Cigliano, Effect of initial aging and high-fat/high-fructose diet on mitochondrial bioenergetics and oxidative status in rat brain, Mol. Neurobiol. 56 (11) (2019) 7651–7663.
[50] L. Yu, X. Dong, X. Xue, S. Xu, X. Zhang, Y. Xu, Z. Wang, Y. Wang, H. Gao, Y. Liang, others, Melatonin attenuates diabetic cardiomyopathy and reduces myocardial vulnerability to ischemia-reperfusion injury by improving mitochondrial quality control: role of SIRT6, J. Pineal Res. (2020), e12698.
[51] C. Gu, T. Li, S. Jiang, Z. Yang, J. Lv, W. Yi, Y. Yang, M. Fang, AMP-activated protein kinase sparks the fire of cardioprotection against myocardial ischemia and cardiac ageing, Ageing Res. Rev. 47 (2018) 168–175.
[52] H. Zhou, Y. Zhang, S. Hu, C. Shi, P. Zhu, Q. Ma, Q. Jin, F. Cao, F. Tian, Y. Chen, Melatonin protects cardiac microvasculature against ischemia/reperfusion injury via suppression of mitochondrial fission-VDAC1-HK2-mPTP-mitophagy axis, J. Pineal Res. 63 (1) (2017), e12413.
[53] X.N. Wang, G.X. Xue, W.C. Liu, H. Shu, M.W. Wang, Y.Y. Sun, X.J. Liu, Y.E. Sun, C. F. Liu, J. Liu, others, Melatonin alleviates lipopolysaccharide-compromised integrity of blood-brain barrier through activating AMP-activated protein kinase in old mice, Aging Cell 16 (2) (2017) 414–421.
[54] K. Sivalingam, T. Cirino, J. McLaughlin, T. Samikkannu, HIV-tat and cocaine impact brain energy metabolism: redox modification and mitochondrial biogenesis influence NRF transcription-mediated neurodegeneration, Mol. Neurobiol. (2020), https://doi.org/10.1007/s12035-020-02131-w.
[55] A. Guo, K. Li, Q. Xiao, Fibroblast growth factor 19 alleviates palmitic acid-induced mitochondrial dysfunction and oxidative stress via the AMPK/PGC-1α pathway in skeletal muscle, Biochem. Biophys. Res. Commun. 526 (4) (2020) 1069–1076.
[56] D. Liu, Z. Ma, L. Xu, X. Zhang, S. Qiao, J. Yuan, PGC1alpha activation by pterostilbene ameliorates acute doxorubicin cardiotoxicity by reducing oxidative stress via enhancing AMPK and SIRT1 cascades, Aging 11 (22) (2019) 10061–10073.
[57] M. Reutzel, R. Grewal, B. Dilberger, C. Silaidos, A. Joppe, G. Eckert, Cerebral mitochondrial function and cognitive performance during aging: a longitudinal study in NMRI mice, Oxidative medicine and cellular longevity 2020 (2020) 4060769.